ACS NANO
Cite This: ACS Nano XXXX, XXX, XXX−XXX
www.acsnano.org

ARTICLE

# Longer-Lasting Electron-Based Microscopy of Single Molecules in Aqueous Medium

Huan Wang,[†,∥] K. Hima Nagamanasa,[†,∥] Ye-Jin Kim,[†,‡] Oh-Hoon Kwon,[†,‡] and Steve Granick*[,†,‡,§]

[†]IBS Center for Soft and Living Matter, Ulsan 44919, South Korea
[‡]Department of Chemistry, UNIST, Ulsan 44919, South Korea
[§]Department of Physics, UNIST, Ulsan 44919, South Korea

Supporting Information

**ABSTRACT:** Use of electron-based microscopy in aqueous media has been held back because aqueous samples tend to suffer from water radiolysis and other chemical degradation caused by the high energy of incident electrons. Here we show that aqueous liquid pockets in graphene liquid cells at room temperature display significantly improved stability when using deuterated water, $D_2O$. Reporting transmission electron microscopy (TEM) experiments based on common imaging conditions, we conclude that use of $D_2O$ outperforms adding radical scavengers to $H_2O$ regardless of imaging details; it increases the lifetime of dissolved organic macromolecules by a factor of 2−5, and it delays by even longer the appearance of radiolysis-induced bubbles, by a factor of time up to 10. We quantify statistically the consequences of minimizing the electron voltage and dose and conclude that the $D_2O$ environment increases sample longevity without noticeable sacrifice of contrast that is critical for direct imaging of weakly scattering organic macromolecules and biomolecules.

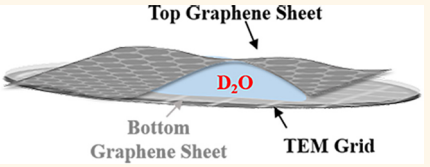


**KEYWORDS:** *liquid-phase TEM, isotope effect, single molecule, beam damage, heavy water, radical scavengers*

Ironically, electron microscopy offers superb single-molecule resolution yet is scarcely used to visualize molecules except in dry or frozen states. It is promising that nanoparticles,[1,2] micelles,[3] and even organic macromolecules[4] can be imaged in real time in liquid media, giving direct information about dynamical rearrangements of shape and structure with better understanding of materials synthesis, electrochemistry, catalysis, and nanoparticle assembly,[5,6] but a severe limitation is damage caused by the incident electrons.[7] Here we are concerned with transmission electron microscopy (TEM).

There are two major impediments to overcoming the difficulties. One is electrical charging from the incident electrons. This can be alleviated by encapsulating pockets of water or aqueous suspension between graphene sheets, which short-circuits charging because graphene is conductive, and enhances signal-to-noise because the graphene sheets and the sample itself are so thin.[2,4,8−10] We consider here the second major impediment, which is chemical degradation caused by the high energy of incident electrons.[5,11] The critical role of the liquid medium itself in influencing radiolysis chemistry became apparent from systematic comparison of times to produce radiolysis-induced bubbles as well as times before visible degradation of single polymer molecules. Experiments were performed across commonly used imaging conditions. Varying the electron acceleration voltage and the electron dosage, our findings are shown to be general. Importantly, in contrast to the common approach of reducing the electron energy, we show quantitatively that tuning the liquid medium, either by adding radical scavengers or even more effectively by using deuterated water, prolongs sample lifetimes without sacrificing contrast that is critical for direct imaging of weak electron-scattering organic molecules in aqueous media.

## RESULTS

**Liquid Pocket Geometry.** We adopt the graphene liquid pocket concept introduced by Alivisatos and co-workers to study nanoparticles in liquid environments (Figure 1A).[2] Our modified method of assembly[4] produces pockets typically rectangular or triangular in cross-section (Figure 1B) with thickness 70−130 nm across the width, estimated by EELS (electron-energy-loss spectroscopy) (Figure S1), consistent with the range 100−300 nm reported by others previously[12] regardless of whether $D_2O$ or $H_2O$ was used (Figure S2). In this community, it is well-known and a subject of much concern that energy injected by electrons promotes water radiolysis that eventually triggers the formation of gas bubbles by radical reactions (Figure 1C).[11,13] All the data in this paper refer to aqueous pockets that were free of gas bubble when the imaging began. Of particular significance is that our experimental parameters included the acceleration voltage 80 keV, which is below the 86 keV threshold above which

Received: June 3, 2018
Accepted: July 13, 2018

Downloaded via ULSAN NATL INST SCIENCE AND TECHLGY on August 7, 2018 at 08:59:18 (UTC).
See https://pubs.acs.org/sharingguidelines for options on how to legitimately share published articles.


© XXXX American Chemical Society

DOI: 10.1021/acsnano.8b04190
ACS Nano XXXX, XXX, XXX−XXX

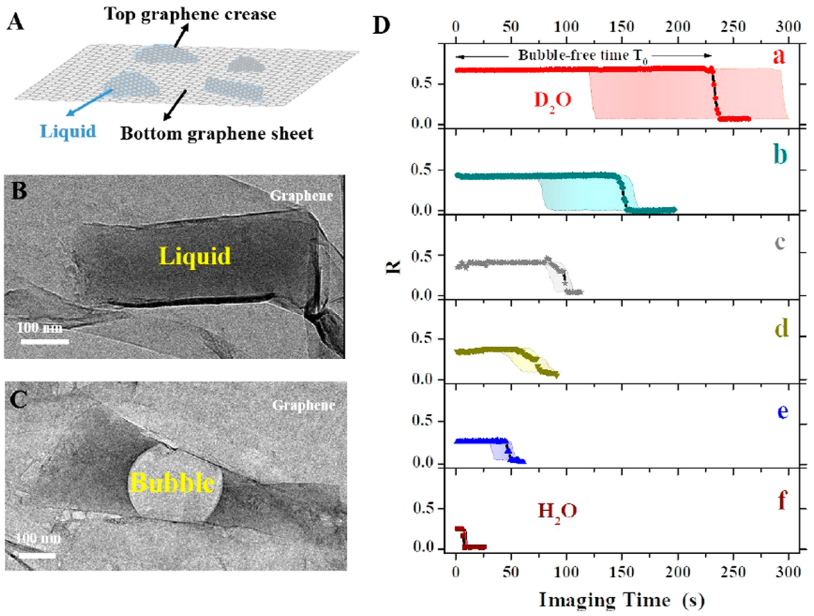


**Figure 1. Experimental scheme and representative data. (A) Schematic diagram of a graphene liquid cell. (B) Representative image when bubble-free; note that the typical shape of graphene liquid pockets is rectangular or triangular. (C) Representative image with a radiation-induced bubble. (D) Normalized contrast *R* plotted against imaging time for representative experiments: plain $D_2O$ (a), plain $H_2O$ (f), and $H_2O$ containing radical scavengers 50% glycerol (b), 100 mM NaCl (c), 10 mM *n*-propyl gallate (d), and 3% glycerol (e). Here *R* is the intensity difference between the sample and a region of graphene just outside the liquid pocket, normalized by the latter. Shaded backgrounds in panel (d) show the variation of bubble onset time in multiple experiments. All data were obtained with 120 keV and dose 22 e $Å^{-2}$ $s^{-1}$.**

electrons can damage graphene by "knock-on" displacement.[14,15]

Contrast stems from the scattering of electrons as they pass through the pocket. For example, as gas bubbles appear and grow, there is less aqueous phase at these positions to scatter them, so electrons are less and less attenuated and the image at these spots appears less dark. Images were taken within 10−15 s including sample focusing and camera initialization time.

**Deuterated Water and Normal Water.** Figure 1D summarizes the large isotope effect that we observed in $D_2O$. Identifying bubbles from contrast at the camera, the normalized contrast is plotted against time of exposure under conditions identified in the caption. The bubble-free time $T_0$ (top panel) is identified from intensity relative to a region of the same graphene sandwich just outside the encapsulated liquid pocket ($R$). Representative raw data are plotted, showing also the range of variation in repeated experiments.

As the bubble-free time in deionized $H_2O$ was only a few seconds (~5 s on average), first we investigated the efficacy of adding radical scavengers, which is a strategy used routinely to prolong sample lifetime from radical-based degradation in fluorescence-based experiments.[16] To work with dearated water was infeasible because when dealing with ~0.5 $\mu$L aqueous solution on a graphene-covered TEM grid, gases in the air will quickly redissolve as the surface-to-volume ratio is so high during the assembly time, ~5 min. In the category of alcohol, glycerol was selected as alcohols scavenge hydroxyl radicals,[17] which are considered to be the major damaging radical to organic materials in liquid phase TEM imaging,[18] and glycerol was selected as it has lower vapor pressure than smaller-molecule alcohols and may help to seal the liquid cell.[19] Compared to plain $H_2O$, this approach prolonged stability by a factor of at least 10: $T_0 \sim 45$ s for 3 wt % glycerol and $T_0 \sim 120$ s for 50 or 70 wt % glycerol. Next, representing the category of small-molecule antioxidants, we considered *n*-propyl gallate (10 mM) as it scavenges singlet oxygen and is reported to be as effective as vitamin C as an antifading agent in fluorescence imaging but at a much lower concentration than vitamin C,[20] and we found $T_0 \sim 90$ s. Also we investigated $H_2O$ containing 100 mM NaCl, not only because NaCl appears to scavenge hydroxyl radicals[21] but especially because of its relevance to conditions of high salt concentration, needed to study nanoparticle growth by in situ TEM[2] and also needed because biological samples such as DNA of course typically require salt buffer to survive. These experiments gave $T_0 \sim 70$ s. Finally, comparing to the case of plain $D_2O$, we found that it was the most long-lived: $T_0 \sim 200$ s on average. Adding radical scavenger to $D_2O$ did not improve lifetime systematically. Otherwise stated, $T_0$ in plain $H_2O$ was extended by alcohol, salt, and *n*-propyl gallate to 50−120 s, probably with different radical scavenging mechanisms in each case, but in plain $D_2O$ it was larger than any of these. Mixtures of 50% $D_2O/H_2O$ extended lifetime qualitatively similar to 50% glycerol/$H_2O$, but deuterated/protiated mixtures were not explored in detail.

Such qualitative differences held regardless of the electron energy or dose rate. From independent experiments and dozens of liquid pockets probed with three different beam conditions, Figure 2 shows the fraction of bubble-containing water pockets plotted against elapsed time in a comparison of $D_2O$ and $H_2O$ with 3% glycerol present to lengthen the lifetime moderately. Data fall into two distinctive distributions according to the liquid content. Almost all $H_2O$ pockets contained some bubbles after ~100 s, but ~75% of the $D_2O$ pockets were free of bubbles after this time and some $D_2O$ pockets persisted free of bubbles for 250 s or longer. Electron energy and dose were second-order influences; milder imaging condition helped but moderately so. Specifically, for the most


DOI: 10.1021/acsnano.8b04190
ACS Nano XXXX, XXX, XXX−XXX

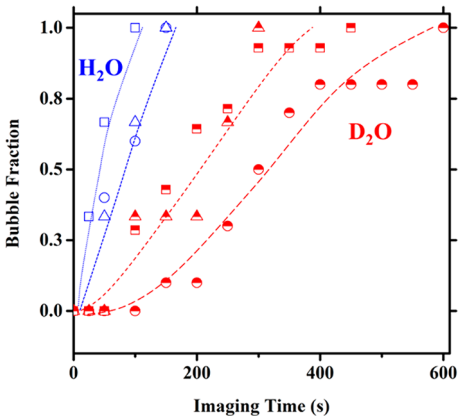


**Figure 2. Comparison of $D_2O$ and $H_2O$. Evaluation of electron energy and electron dose rate regarding retardation of radiolysis-induced bubbles. From multiple experiments, the fraction of liquid pockets containing bubbles is plotted against imaging time for $D_2O$ (red symbols) and $H_2O$ with 3% glycerol (blue symbols). Most extreme radiation: 120 keV and 22 e $Å^{-2}$ $s^{-1}$ (squares). Intermediate radiation: 120 keV and 1.7−5 e $Å^{-2}$ $s^{-1}$ (triangles). Mildest radiation: 80 keV and 1.7−5 e $Å^{-2}$ $s^{-1}$ (circles). Sample size: 14, 6, 10 and 3, 6, 5 for $D_2O$ and $H_2O$ under these respective conditions. Curved dotted lines are guides to the eye only.**

extreme condition of 120 keV, 22 e $Å^{-2}$ $s^{-1}$, ∼60% of $D_2O$ pockets remained free of bubble after ∼150 s, while almost all $H_2O$ pockets acquired bubbles even probed with the mildest electron beam, 80 keV, 1.7−5 e $Å^{-2}$ $s^{-1}$. Interestingly, unlike what one might have expected, graphene "knock-on" energy did not seem present a threshold of systematic significant damage, as indicated specially by the indistinguishable two data sets of $D_2O$ of the same dose but different voltages, 120 and 80 keV. Note that the bubble onset time did not correlate with width of the liquid pocket.

Likewise, the rate of bubble growth was slower in $D_2O$. In the literature, most liquid-phase TEM measurements are made using electron energy at least 120 keV, so this aspect was investigated at 120 keV and the highest electron dose rate, 22 e $Å^{-2}$ $s^{-1}$, that we considered. Dozens of repeated experiments were made. In a typical experiment, there appeared in each pocket just one bubble and its growth rate fluctuated; the average growth rates were ∼1300 $nm^2$/s and ∼900 $nm^2$/s in $H_2O$ and $D_2O$, respectively (Figure S3). Whereas the growth rate for $H_2O$ had a similar order of magnitude to that reported by others under similar electron beam conditions though using $SiN_x$ windows,[13] in $D_2O$ it was consistently less.

Putting these findings into perspective, we emphasize that while potential experimental concerns (possibly the actual purity of water or disputable salt residue within graphene liquid pockets) might indeed in principle contribute to any given experiment, they do not appear to modify the significant statistical differences, between $D_2O$ and $H_2O$, that we report from a large statistical data set.

**Radiation Damage of Dissolved Polyelectrolyte in $D_2O$.** Especially when the electron voltage was low, these differences correlated with longer lifetimes of our model system, dissolved aqueous polystyrenesulfonate. Our measure of chemical degradation was visible bond scission. EELS and EDX (energy dispersive X-ray spectroscopy) mapping confirmed the presence of sulfur from this molecule within the pockets (Figure S4).

Figure 3A tabulates the lifetimes of individual molecules from numerous independent experiments. Relative to $H_2O$

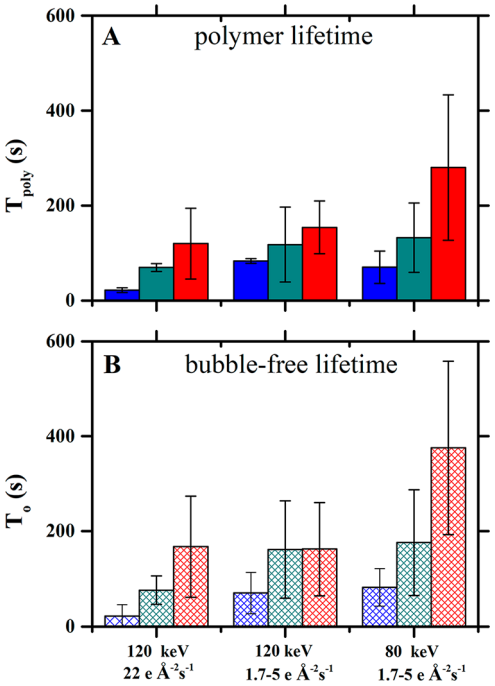


**Figure 3. Comparison of polymer lifetime and liquid bubble-free time. Comparison of $D_2O$ and $H_2O$, electron energy, and electron dose rate, regarding (A) lifetime of high-molecular-weight polystyrenesulfonate and (B) bubble-free lifetime in liquid pockets free of solute under the same conditions, for plain $D_2O$ (red), $H_2O$ with 3% glycerol (blue), and $H_2O$ with 50% glycerol (green). The abscissa of this bar graph shows the conditions of electron energy and dose rate: Most extreme radiation: 120 keV and 22 e $Å^{-2}$ $s^{-1}$. Intermediate radiation: 120 keV and 1.7−5 e $Å^{-2}$ $s^{-1}$. Mildest radiation: 80 keV and 1.7−5 e $Å^{-2}$ $s^{-1}$. Sample size: 14, 6, 10; 14, 6, 11; and 3, 6, 5 for $D_2O$, $H_2O$ with 50% glycerol, and $H_2O$.**

containing 3% glycerol as antioxidant, the mean lifetime in $D_2O$ was longer, ∼1.3−2 times longer than even 50% glycerol/$H_2O$, the most effective radical scavenging system that we surveyed. So long as the liquid pocket remained free of bubbles, the mean lifetime was ∼260 s, in fact as long as 400 s in some cases, under the mildest conditions (80 keV electrons and dose rate 1.7−5 e $Å^{-2}$ $s^{-1}$). Likewise, the dependence of liquid pocket bubble-free lifetime on electron energy and dose followed these same trends (Figure 3B). Movie S1 emphasizes this useful contrast between $D_2O$ and $H_2O$.

The polymer lifetime was consistently less than the bubble-free time, suggesting that there may exist a threshold concentration of accumulated radiolytic products needed to cause chain scission (Figure 4). To quantify this, we computed the projected size of the polystyrenesulfonate macromolecules that we imaged, finding this to fluctuate (±3%) around the same stable value at first, but followed by relatively sudden size reduction and faded contrast (>5%). In executing this comparison, we normalized to the background without macromolecule present and also to the image of the macromolecule at time zero. Typically, such molecules ceased to be visible within ∼10 s after the onset of this visible degradation and a bubble appeared soon afterward. The process was qualitatively similar in $D_2O$ (Figure 4A, upper


DOI: 10.1021/acsnano.8b04190
ACS Nano XXXX, XXX, XXX−XXX

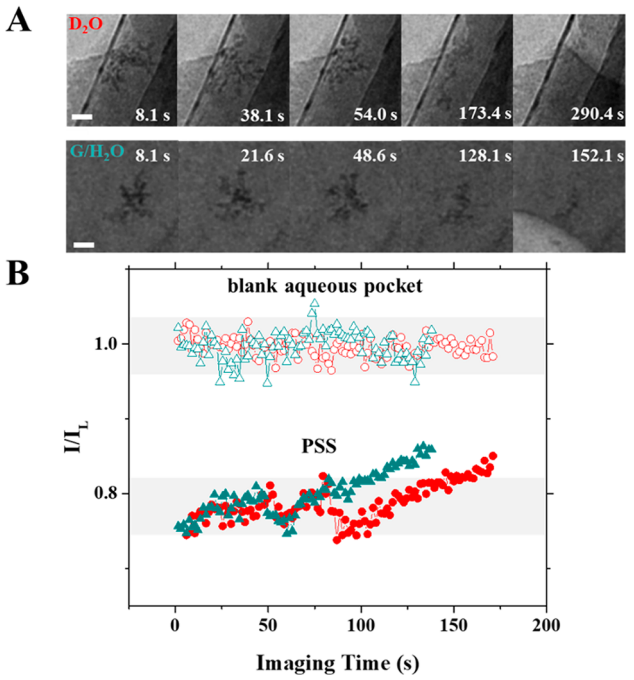


**Figure 4. Beam-induced degradation of dissolved polymer precedes radiolysis-induced bubble. In these two experiments, bubbles were first observed at elapsed time 290 s ($D_2O$) and 152 s (glycerol/$H_2O$). (A) Representative images of polystyrenesulfonate (PSS) before bubbles appeared, at times indicated next to each image. Scale bar is 20 nm. (B) Plots of intensity I relative to blank liquid $I_L$ versus imaging time: comparison of polymer contrast and degradation in $D_2O$ (circles) and 50% glycerol/$H_2O$ (triangles). Intensity at the camera, quantified as described elsewhere,[4] and its ratio to surrounding liquid background, defined as contrast, are plotted against imaging time. Blank aqueous pocket intensity (open symbols), normalized to $t$ = 0, is shown for comparison. Gray shaded region indicates normal fluctuation range and is a guide to the eye.**

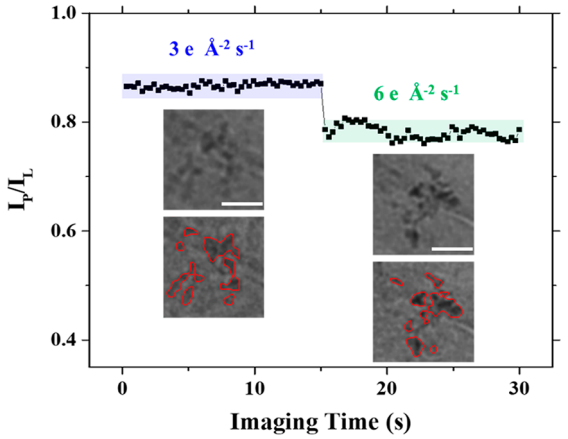


**Figure 5. Dependence of polymer contrast on electron dosage in $D_2O$. Contrast, defined as the ratio of average intensity per pixel within the polymer image, $I_P$, to the average intensity per pixel in the surrounding aqueous medium, $I_L$, is plotted against time during an experiment in which the electron dose was switched midway through the experiment: 3 e Å$^{-2}$ s$^{-1}$, from 0 to 15 s, then 6 e Å$^{-2}$ s$^{-1}$. Shaded region indicate normal fluctuation range. Scale bar is 20 nm. Insets show representative images taken with 0.3 s exposure with continuous capture at 80 keV during each time period. These raw images of weakly adsorbed polymer random coils (top frame) are accompanied by features identified from image analysis[4] (bottom frame). These images fluctuate with time reflecting conformational fluctuations. The improved contrast at high electron dose. Minimal electron damage is suggested by the fact that $I_P/I_L$ fluctuates about a constant level.**

panel) and $H_2O$ (50% glycerol, Figure 4A, lower panel) though the lifetime in pure $D_2O$ was much longer (Movie S2).

It is reasonable to anticipate that radiolysis began starting from the first exposure to high-energy electrons at the start of any experiment. This is consistent with the observation (Figure 4B) that the intensity of electrons impinging on the detection camera usually increased in slow linear fashion on top of flickering fluctuations with time during the bubble-free period (up to ~5%), although we present no quantitative explanation at this time. Additional experiments employing quantitative EELS to differentiate free sulfur in solution and bound sulfur on polymer in situ will help to understand mechanism and kinetics of polymer degradation, however to accomplish this will be extremely difficult given the fragility of our sample under the long necessary exposure to focused high energy (200 keV) STEM beam, these conditions being required to resolve single molecules. Subtle structural changes such as breakage of a single bond would be beyond our resolving capability.

Taken together, our observations suggest that the absence of radiolysis-induced gas bubbles was accompanied by relatively safe conditions in which to image this macromolecule. While polymer contrast was improved when at constant 80 keV energy the electron dosage was increased (Figure 5), the effect of raising the voltage from 80 to 120 keV was insignificant, buried within the statistical variance between samples (these differences probably originate in different liquid-cell thickness and some variability between the solid supports on which pockets are formed). That polymer contrast was systematically better within liquid pockets of graphene suspended on holes than on carbon film, and better on single sheet graphene than on graphene folds, can be useful to experimentalists (Figure 4A, upper panel).

It seems there is a sweet spot in which sample lifetime is extended significantly while maintaining a satisfactory level of image contrast. First, reduced electron dosage at constant 120 keV voltage, from 22 to 1.7−5 e Å$^{-2}$ s$^{-1}$ (Figure 3A), prolonged the lifetime of dissolved PSS by a factor of 3, for both $D_2O$ and $H_2O$. Second, use of $D_2O$ increased the dissolved PSS lifetime 2−5 times under these same imaging conditions. Third, polymer contrast was the same regardless of using $H_2O$ or $D_2O$ (Figure 4). Fourth, 2-fold decrease of electron dose, from 6 to 3 e Å$^{-2}$ s$^{-1}$, came at the expense of only 10% polymer contrast decrease in $D_2O$ (Figure 5). Usually there is a trade-off between prolonged lifetime, produced by decreasing the electron dose, and enhanced contrast, produced by increasing the electron dose. Taken together, the present findings show that $D_2O$ liquid medium prolongs imaging lifetime while retaining needed contrast.

## DISCUSSION

Isotope differences between $D_2O$ and $H_2O$ are well-known regarding other physical properties (density, viscosity, melting point, hydrogen bonding, for example[22,23]) and have been exploited to enable many characterization methods (neutron scattering, NMR, infrared, fluorescence and Raman imaging, solution reaction kinetics, for example).[24,25] The findings


DOI: 10.1021/acsnano.8b04190
ACS Nano XXXX, XXX, XXX−XXX

reported here are physically reasonable and can be practically useful to experimentalists.

Considering the initial process of radiolysis that splits a water molecule into H· and ·OH radicals, it is clear that electrons must collide with water inelastically and transfer kinetic energy to it. The higher mass of neutrons in D· radicals makes them more difficult than H· to knock off. Indeed, according to the 79 reactions that have been considered to contribute to the radiolysis of water all except one of them require the H· radical to be present.[11] This is also consistent with our observation that whereas dose rate matters more for $H_2O$, electron energy matters more for $D_2O$ (Figure 2). Similarly, the reaction kinetics of bimolecular $D_2$ formation from D· would be retarded by the same degree as compared to $H_2$ formation from H·. Therefore, one should anticipate that $D_2$ gas takes longer to form than $H_2$, and that as this gas is the major constituent of radiolytically formed gas bubbles, bubble formation in $D_2O$ should be retarded. Moreover, as radicals containing D are generally less reactive than their counterparts of lower mass, slower cascade reactions to generate other gaseous products such as $O_2$ are anticipated.[26,27]

To the extent that the root cause of our findings may be a bulk effect, it is relevant that, in response to high-energy gamma ray radiation, radiolysis of $D_2O$ is slower than $H_2O$ by a factor of ∼1.1 to ∼1.5,[28,29] which implies a higher steady-state concentration of $H_2$ gas than $D_2$ gas. This we confirmed by running the same simulation of kinetic equations reported by others[11] except with G values (a number to quantify the sensitivity of organic materials to radiation) more appropriate to the conditions of these experiments (Figure S5). This can be taken only as suggestive, however, given the large energy differences between gamma-ray and electron-induced radiolysis; relevant parameters for electron-induced radiolysis are not yet known, to the best of our knowledge. Independently, coarse-grained quantification of gas bubble growth echoed a similar difference (Figure S3), although the nonlinear nature of growth kinetics was not taken into account. Solubility differences may contribute, as $D_2$ gas has higher solubility in $D_2O$ than $H_2$ in $H_2O$ by a factor of 1.3 at room temperature[30−33] which is believed to be the relevant comparison since electron-induced heating is believed to be at most several degrees.[13] At the same time, temperature may play a role as the thermal conductivity coefficient of liquid $D_2O$ is larger than of $H_2O$.[34] This should assist heat dissipation and may contribute to our observation as usually gas solubility ($H_2$ or $D_2$) decreases as temperature increases.[33] In addition to bulk effects, surface effects may contribute to our observations. Though graphene has low surface energy, inevitably it carries adsorbed gases when specimens are prepared in the ambient laboratory environment. The large surface-to-volume ratio in a graphene liquid cell may contribute to the statistical variability that here we report. Collectively, these considerations regarding bulk and surface effects suggest that these multiple reasons can produce the same empirical observation that the isotope effect appears to retard radical reactions significantly.

Regarding an isotope effect on lifetime of organic molecules in the presence of high-energy electrons, absence of liquids, the accumulation of energy in individual bonds may contribute as deuterated organic molecules have been reported to withstand ∼2× longer radiation exposure than their lighter counterparts simply due to the difference in knock-on energy.[35] From the perspective of chemical intuition, it is clear that chain scission of our organic polymer depended ultimately on strength of individual C−C bonds in their aqueous environment, but this matter is complex as it involves modeling the mechanism of energy transfer between molecule and its aqueous environment, and it is not realistic to attempt to do so at this time. Nonetheless, it has been shown that deuterating DNA causes it to resist hydroxyl radical damage in solution as this slows hydrogen abstraction from the sugar backbone.[36]

## CONCLUSION

We conclude with hopefulness that these methods to extend sample lifetime in liquid-cell TEM microscopy can be useful to experimentalists. The main point is practical: replacing $H_2O$ by $D_2O$ reduces significantly electron beam damage in graphene liquid pockets not only by extending the sample lifetime of the organic macromolecule that we studied, but also by prolonging the time for onset of gas bubbles whose agitation would disturb samples of interest, at no appreciable expense of contrast. Among the possible reasons surveyed here, no ranking is attempted at this time which ones dominate, but probably all of them contribute. For scientists interested in liquid-phase electron microscopy of radiation-sensitive synthetic polymers and biopolymers, these findings can be useful.

## MATERIALS AND METHODS

**Preparation of Graphene Liquid Pockets.** Our liquid pockets are formed by creases that we create with care when one graphene sheet is laid as a sandwich on top of another that traps the liquid.[4] Specifically, we first transfer commercial CVD grown graphene/Cu (ACS Materials) onto a holey carbon gold TEM grid (QUANTIFOIL, Electron Microscopy Sciences and SPI Supplies), followed by micropipetting a relatively large liquid volume (about 0.5 μL) to maximize the chances to form multiple liquid pockets. Quickly and gently, using tweezers, we place the droplet-bearing, graphene-coated grid onto a graphene sheet that floats on a copper etchant solution, 0.1 M $(NH_4)_2S_2O_8$, and leave it for a few min for graphene sheets to adhere strongly to encapsulate the sample liquid between creases. Reagents (Sigma-Aldrich) were purchased with the highest purity available and used as received. $H_2O$ used was produced from Millpore, with resistivity 18.2 MΩ cm.

**Electron Microscopes.** Many of our TEM experiments were performed using an instrument of the kind routinely available at many research institutions: JEOL-1400 in the Central Research Facilities at our university, with 120 keV electron energy and dose rate 22 e $Å^{-2}$ $s^{-1}$ similar to parameters used by other researchers to study dynamics with this technique,[3,8] such that images were collected consecutively with 0.3 s exposure time and 1 s between frames. In other TEM experiments, we used a JEOL-2100 TEM equipped with a direct electron-detection camera with single-electron sensitivity (K2 Summit, Gatan)[37] with temporal resolution of 0.3 s and no lag between frames, thus allowing us to explore systematically the influences of electron energy and dose rate (120 keV, 22 e $Å^{-2}$ $s^{-1}$; 120 keV, 1.7−5 e $Å^{-2}$ $s^{-1}$; and 80 keV, 1.7−5 e $Å^{-2}$ $s^{-1}$).

**Electron Energy Loss Spectroscopy (EELS) and Energy Dispersive X-ray Spectroscopy (EDXS).** Electron energy loss spectra of water pockets were taken with a JEOL-2100 transmission electron microscope using a CCD camera (US4000, Gatan) at 120 keV, less than 10 mrad collection semiangle, and 5 s exposure time.

**Simulations of $D_2$ and $H_2$ Production Rate.** The kinetic rate equations[11] and open-source Matlab codes introduced by Elliot and McCracken[38] were used.

**Organic Polymer.** The polystyrenesulfonate had weight-average molar mass $M_w$ = 2200 kDa and ratio of weight-average to number-average molecular weight $M_w/M_n$ = 1.15) (Polymer Source).[4] After solutions were prepared at 1 wt % concentration and equilibrated for 24 h ($D_2O$ included, allowing hydrogen to exchange with deterium), graphene-cell liquid pockets containing this polymer were prepared.



DOI: 10.1021/acsnano.8b04190
ACS Nano XXXX, XXX, XXX−XXX

## ASSOCIATED CONTENT

### Supporting Information

The Supporting Information is available free of charge on the ACS Publications website at DOI: 10.1021/acsnano.8b04190.

Additional data and figures (PDF)

Side-by-side comparison of polystyrenesulfonate in liquid pockets with $D_2O$ and $H_2O$ (3% glycerol); accelerating voltage is 120 keV, and dose rate is 22 e $Å^{-2}$ $s^{-1}$ (AVI)

Side-by-side comparison of polystyrenesulfonate contrast and lifetime in liquid pockets with $D_2O$ and $H_2O$ (50% glycerol); accelerating voltage is 80 keV, and dose rate is 1.7−5 e $Å^{-2}$ $s^{-1}$ (AVI)

Dependence of polystyrenesulfonate contrast on electron dose; accelerating voltage is 80 keV, and dose rate is 3 e $Å^{-2}$ $s^{-1}$ from 0 to 15 s and increased to 6 e $Å^{-2}$ $s^{-1}$ thereafter (AVI)

## AUTHOR INFORMATION


### Corresponding Author

*E-mail: sgranick@ibs.re.kr.

### ORCID

Steve Granick: 0000-0003-4775-2202


### Author Contributions

‖H.W. and K.H.N. contributed equally.


### Funding

We thank taxpayers who supported this work through the Korean Institute for Basic Science, Project Code IBS-R020-D1.


### Notes

The authors declare no competing financial interest.


## ACKNOWLEDGMENTS

For discussions, we are indebted to Cong Xu.


## REFERENCES


(1) Zheng, H.; Smith, R. K.; Jun, Y.-w.; Kisielowski, C.; Dahmen, U.; Alivisatos, A. P. Observation of Single Colloidal Platinum Nanocrystal Growth Trajectories. *Science* **2009**, *324*, 1309−1312.

(2) Yuk, J. M.; Park, J.; Ercius, P.; Kim, K.; Hellebusch, D. J.; Crommie, M. F.; Lee, J. Y.; Zettl, A.; Alivisatos, A. P. High-resolution EM of Colloidal Nanocrystal Growth using Graphene Liquid Cells. *Science* **2012**, *336*, 61−64.

(3) Parent, L. R.; Bakalis, E.; Ramírez-Hernández, A.; Kammeyer, J. K.; Park, C.; de Pablo, J.; Zerbetto, F.; Patterson, J. P.; Gianneschi, N. C. Directly Observing Micelle Fusion and Growth in Solution by Liquid-Cell Transmission Electron Microscopy. *J. Am. Chem. Soc.* **2017**, *139*, 17140−17151.

(4) Nagamanasa, K. H.; Wang, H.; Granick, S. Liquid-Cell Electron Microscopy of Adsorbed Polymers. *Adv. Mater.* **2017**, *29*, 1703555.

(5) Ross, F. M. Opportunities and Challenges in Liquid Cell Electron Microscopy. *Science* **2015**, *350*, AAA9886.

(6) Liao, H. G.; Zheng, H. Liquid Cell Transmission Electron Microscopy. *Annu. Rev. Phys. Chem.* **2016**, *67*, 719−747.

(7) Guo, C.; Allen, F. I.; Lee, Y.; Le, T. P.; Song, C.; Ciston, J.; Minor, A. M.; Gomez, E. D. Probing Local Electronic Transitions in Organic Semiconductors through Energy-Loss Spectrum Imaging in the Transmission Electron Microscope. *Adv. Funct. Mater.* **2015**, *25*, 6071−6076.

(8) Chen, Q.; Smith, J. M.; Park, J.; Kim, K.; Ho, D.; Rasool, H. I.; Zettl, A.; Alivisatos, A. P. 3D motion of DNA-Au Nanoconjugates in Graphene Liquid Cell Electron Microscopy. *Nano Lett.* **2013**, *13*, 4556−4561.

(9) Park, J.; Park, H.; Ercius, P.; Pegoraro, A. F.; Xu, C.; Kim, J. W.; Han, S. H.; Weitz, D. A. Direct Observation of Wet Biological Samples by Graphene Liquid Cell Transmission Electron Microscopy. *Nano Lett.* **2015**, *15*, 4737−4744.

(10) Wang, C.; Shokuhfar, T.; Klie, R. F. Precise *in situ* Modulation of Local Liquid Chemistry *via* Electron Irradiation in Nanoreactors based on Graphene Liquid Cells. *Adv. Mater.* **2016**, *28*, 7716−7722.

(11) Schneider, N. M.; Norton, M. M.; Mendel, B. J.; Grogan, J. M.; Ross, F. M.; Bau, H. H. Electron−Water Interactions and Implications for Liquid Cell Electron Microscopy. *J. Phys. Chem. C* **2014**, *118*, 22373−22382.

(12) Sasaki, Y.; Kitaura, R.; Yuk, J. M.; Zettl, A.; Shinohara, H. Efficient Preparation of Graphene Liquid Cell Utilizing Direct Transfer with Large-Area Well-Stitched Graphene. *Chem. Phys. Lett.* **2016**, *650*, 107−112.

(13) Grogan, J. M.; Schneider, N. M.; Ross, F. M.; Bau, H. H. Bubble and Pattern Formation in Liquid Induced by An Electron Beam. *Nano Lett.* **2014**, *14*, 359−364.

(14) Smith, B. W.; Luzzi, D. E. Electron Irradiation Effects in Single Wall Carbon Nanotubes. *J. Appl. Phys.* **2001**, *90*, 3509−3515.

(15) Meyer, J. C.; Eder, F.; Kurasch, S.; Skakalova, V.; Kotakoski, J.; Park, H. J.; Roth, S.; Chuvilin, A.; Eyhusen, S.; Benner, G.; Krasheninnikov, A. V.; Kaiser, U. Accurate Measurement of Electron Beam Induced Displacement Cross Sections for Single-Layer Graphene. *Phys. Rev. Lett.* **2012**, *108*, 196102.

(16) Rasnik, I.; McKinney, S. A.; Ha, T. Nonblinking and Long-Lasting Single-Molecule Fluorescence Imaging. *Nat. Methods* **2006**, *3*, 891−893.

(17) Rosenblum, W. I.; El-Sabban, F. Dimethyl Sulfoxide (DMSO) and Glycerol, Hydroxyl Radical Scavengers, Impair Platelet Aggregation within and Eliminate the Accompanying Vasodilation of Injured Mouse Pial Arterioles. *Stroke* **1982**, *13*, 35−39.

(18) Cho, H.; Jones, M. R.; Nguyen, S. C.; Hauwiller, M. R.; Zettl, A.; Alivisatos, A. P. The Use of Graphene and Its Derivatives for Liquid-Phase Transmission Electron Microscopy of Radiation-Sensitive Specimens. *Nano Lett.* **2017**, *17*, 414−420.

(19) Woehl, T. J.; Jungjohann, K. L.; Evans, J. E.; Arslan, I.; Ristenpart, W. D.; Browning, N. D. Experimental Procedures to Mitigate Electron Beam Induced Artifacts During *In Situ* Fluid Imaging of Nanomaterials. *Ultramicroscopy* **2013**, *127*, 53−63.

(20) Aitken, C. E.; Marshall, R. A.; Puglisi, J. D. An Oxygen Scavenging System for Improvement of Dye Stability in Single-Molecule Fluorescence Experiments. *Biophys. J.* **2008**, *94*, 1826−1835.

(21) Atinault, E.; De Waele, V.; Schmidhammer, U.; Fattahi, M.; Mostafavi, M. Scavenging of e and OH Radicals in Concentrated HCl and NaCl Aqueous Solutions. *Chem. Phys. Lett.* **2008**, *460*, 461−465.

(22) Guillot, B.; Guissani, Y. Hydrogen-Bonding in Light and Heavy Water under Normal and Extreme Conditions. *Fluid Phase Equilib.* **1998**, *150−151*, 19−32.

(23) Scheiner, S.; Čuma, M. Relative Stability of Hydrogen and Deuterium Bonds. *J. Am. Chem. Soc.* **1996**, *118*, 1511−1521.

(24) Sukhishvili, S. A.; Granick, S. Layered, Erasable Polymer Multilayers Formed by Hydrogen-Bonded Sequential Self-Assembly. *Macromolecules* **2002**, *35*, 301−310.

(25) Mudalige, A.; Pemberton, J. E. Raman Spectroscopy of Glycerol/D2O Solutions. *Vib. Spectrosc.* **2007**, *45*, 27−35.

(26) Gierczak, T.; Talukdar, R. K.; Herndon, S. C.; Vaghjiani, G. L.; Ravishankara, A. R. Rate Coefficients for the Reactions of Hydroxyl Radicals with Methane and Deuterated Methanes. *J. Phys. Chem. A* **1997**, *101*, 3125−3134.

(27) Shafirovich, V.; Dourandin, A.; Luneva, N. P.; Geacintov, N. E. The Kinetic Deuterium Isotope Effect as a Probe of a Proton Coupled Electron Transfer Mechanism in the Oxidation of Guanine by 2-Aminopurine Radicals. *J. Phys. Chem. B* **2000**, *104*, 137−139.

(28) Hayon, E. Radiolysis of Heavy Water in the pD Range 0−14. *J. Phys. Chem.* **1965**, *69*, 2628−2632.

(29) Elliot, A. J.; Chenier, M. P.; Ouellette, D. C. Temperature Dependence of G Values for H2O and D2O Irradiated with Low




DOI: 10.1021/acsnano.8b04190
*ACS Nano* XXXX, XXX, XXX−XXX

Linear Energy Transfer Radiation. *J. Chem. Soc., Faraday Trans.* **1993**, *89*, 1193−1197.
(30) Prini, R. F.; Crovetto, R. Evaluation of Data on Solubility of Simple Apolar Gases in Light and Heavy Water at High Temperature. *J. Phys. Chem. Ref. Data* **1989**, *18*, 1231−1243.
(31) Scharlin, P.; Battino, R. Solubility of 13 Nonpolar Gases in Deuterium Oxide at 15 - 45∼ and 101.325 kPa. Thermodynamics of Transfer of Nonpolar Gases from H2O to D2O. *J. Solution Chem.* **1992**, *21*, 67−91.
(32) Fernández-Prini, R.; Alvarez, J. L.; Harvey, A. H. Henry's Constants and Vapor−liquid Distribution Constants for Gaseous Solutes in H2O and D2O at High Temperatures. *J. Phys. Chem. Ref. Data* **2003**, *32*, 903−916.
(33) Setthanan, U.; Morris, D. R.; Lister, D. H. Solubilities of H2 in H2O and D2 in D2O with Dissolved Boric Acid and Lithium Hydroxide. *Can. J. Chem.* **2006**, *84*, 65−68.
(34) Le Neindre, B.; Bury, P.; Tufeu, R.; Vodar, B. Thermal Conductivity Coefficients of Water and Heavy Water in the Liquid State up to 370 degree C. *J. Chem. Eng. Data* **1976**, *21*, 265−274.
(35) Chamberlain, T. W.; Biskupek, J.; Skowron, S. T.; Bayliss, P. A.; Bichoutskaia, E.; Kaiser, U.; Khlobystov, A. N. Isotope Substitution Extends the Lifetime of Organic Molecules in Transmission Electron Microscopy. *Small* **2015**, *11*, 622−629.
(36) Balasubramanian, B.; Pogozelski, W. K.; Tullius, T. D. DNA Strand Breaking by the Hydroxyl Radical is Governed by the Accessible Surface Areas of the Hydrogen Atoms of the DNA Backbone. *Proc. Natl. Acad. Sci. U. S. A.* **1998**, *95*, 9738−9743.
(37) Lee, Y. M.; Kim, Y. J.; Kim, Y.-J.; Kwon, O.-H. Ultrafast Electron Microscopy Integrated with A Direct Electron Detection Camera. *Struct. Dyn.* **2017**, *4*, 044023.
(38) Elliot, A. J.; McCracken, D. R. Computer Modelling of the Radiolysis in An Aqueous Lithium Salt Blanket: Suppression of Radiolysis by Addition of Hydrogen. *Fusion Eng. Des.* **1990**, *13*, 21−27.



DOI: 10.1021/acsnano.8b04190
*ACS Nano* XXXX, XXX, XXX−XXX